Korean J. Chem. Eng., **28**(3), 939-948 (2011)
DOI: 10.1007/s11814-010-0423-0

Modifying GMA equation of state for description of (P, ρ, T) relation of gas and liquids over an extended pressure range

Mehdi Baniasadi*,, Sattar Ghader*,†, and Hassan Hashemipour***

*Department of Chemical Engineering, College of Engineering, Shahid Bahonar University of Kerman, Jomhoori blvd., Post Code 76175, Kerman, Iran
**Young Researchers Society, Shahid Bahonar University of Kerman, Post Code 76175, Kerman, Iran
(*Received 22 July 2010 • accepted 6 September 2010*)

Abstract−The main concern of this paper is on the improvement of the GMA equation of state (Fluid Phase Equilibr. 230 (2005) 170) which has been used for density calculation of components in liquid region with excellent accuracy. However, the GMA equation of state cannot predict the density of components in either the gas or gas-liquid transition region. The GMA equation of state is based on intermolecular potential energy; therefore, the potential energy of the GMA equation of state is corrected and an equation of state is obtained. The final form of the new equation of state is a regularity between $(Z-1)v^3$ and ρ for all temperatures, which is based on modified Lennard-Jones potential (9, 6, 3). The capability of the new equation of state is examined by comparing the results with experimental data in homogeneous gas, homogeneous liquid and gas-liquid transition region from low to very high pressures. The new equation of state gives excellent results in homogeneous gas and homogeneous liquid region, while the predictions in the gas-liquid transition have more deviations. The average absolute deviation between calculated and experimental densities for 1979 data points of 24 components is 0.25% over the entire range of data with a maximum pressure of 1,000 MPa.

Key words: Density, Isotherm Regularity, GMA Equation of State, High Pressure

INTRODUCTION

Physical and thermodynamic data of various chemical components at low and high pressures are required for efficient design and operation of chemical industries. For example, compressed polar fluids are used as media for chemical reactions, separation processes and heat transfer agents, and (P, ρ, T) data of such fluids are required for many chemical process calculations, plant simulations and theoretical evaluation of models. Process variables such as internal energy, enthalpy and entropy are also calculated by equations relating temperature, pressure, density and heat capacity. Density is also a physical property required in several design problems, including sizing of storage vessels, design of equipment and material and energy balances. This property is usually measured and many experimental data are available, and as mentioned they are used in many fields. For example, Hwang et al. [1] performed experiments by supercritical CO_2 at high pressure to study extractions of hexadecane and crude oil. The extraction yields increased as CO_2 density increased with a pressure rise at constant temperature. Also, Lim et al. [2] measured high pressure data for the binary mixtures of CO_2+n-butanol at various isotherms and compared their experimental data with literature. Several equations of state have been derived for predicting densities of gases or liquids, but there are a few satisfactory equations of state (EOS) for the calculations of these properties for gases and liquids simultaneously up to high pressures.

GMA EOS is based on isotherm regularity; therefore, some of works on isotherm regularity are pointed out below. Parsafar and Mason [3] introduced an analytical EOS based on intermolecular potential energy, which is named linear isotherm regularity (LIR). The LIR assumes that $(Z-1)v^2$ varies linearly with ρ^2, where v is molar volume, ρ is molar density, P is pressure, R is universal gas constant, T is temperature and $Z=P/\rho RT$ is the compressibility factor. In derivation of LIR EOS the Lennard-Jones (12, 6) potential energy is used. In other work, Ghatee et al. [4] derived an EOS for liquid cesium over the whole liquid range. This EOS assumes that $(Z-1)v^2$ is a linear function of $1/\rho$ at constant temperature. Recently, a new isotherm regularity based EOS was derived by Goharshadi et al., which is named GMA EOS [5-10]. GMA EOS is an excellent equation for density calculation of liquids at low and high pressures. The GMA EOS considers that a linear relation exists between $(2Z-1)v^3$ and ρ for each isotherm. This EOS has not been applied for density calculation of components in the gas region.

In this work an EOS is proposed that considers potential energy among the molecules. The objective of this work was to improve the potential energy based EOS, namely GMA, by adding a specific term to take into account interactions in gas phase and gas-liquid transition region. The general aim was to develop a correlative tool applicable under different states of liquid, gas and gas-liquid transition for density calculation specifically at high pressure. Once the EOS was improved, its application to experimental data has covered some polar and nonpolar components at different states, and density at various temperatures and pressures (low and high) is calculated, proving its validity in most of the cases.

THEORY (EOS DETAILS)

The GMA EOS [5-10] assumes

†To whom correspondence should be addressed.
E-mail: sattarghader@yahoo.com

$$(2Z-1)v^3=A(T)+B(T)\rho \quad (1)$$

which shows a linear relation should exist between $(2Z-1)v^3$ and ρ for the component in concern for all isotherms where A and B are temperature-dependent parameters. Goharshadi et al. verified this regularity for many liquids and obtained very accurate calculation of liquid density at low and high pressure [5-10]. The A and B parameters are determined by correlating experimental data in the form of Eq. (1), and therefore the EOS is correlative type. We have tested this EOS for gases using experimental data and found that the linear relation between $(2Z-1)v^3$ and ρ does not exist for any of gases. Therefore, we devised a way to improve this EOS and present a new regularity EOS in terms of the potential energy for gases and liquids that can be used for calculation of gas and liquids density. The EOS is indeed based on the correlation of experimental data like GMA EOS, but it is based on a different regularity. The potential energy used in GMA EOS is $U=(N/2)Z[(c_9/r^9)-(c_6/r^6)]$, where U is the total potential energy in N molecules and z is coordination number. The potential energy of the GMA equation of state is corrected and an equation of state is obtained.

For obtaining a new EOS we begin with the exact thermodynamic relation (like the method used for GMA EOS derivation in refs. 5-10):

$$P=T\left(\frac{\partial P}{\partial T}\right)_{\rho}-\left(\frac{\partial u}{\partial v}\right)_{T} \quad (2)$$

where the first and second terms of Eq. (2) are called the thermal and internal pressures (P_i). In this work, we used a modified Lennard-Jones potential (9, 6, 3) for potential energy with temperature-dependent coefficients:

$$U=\frac{N}{2}z\left(\frac{C_9}{r^9}+\frac{C_6}{r^6}+\frac{C_3}{r^3}\right) \quad (3)$$

where N is number of molecules and C_i are coefficients of potential energy which are assumed to be temperature dependent. z is the coordination number which is supposed independent of density, and r is the distance among molecules. A motivation for this form is that it yields an EOS which is an extension of GMA EOS. Physically, terms proportional to r^{-6} and r^{-9} can be justified in potential energy because a dispersion interaction, together with a term representing the repulsive interactions, is expected to be present for molecules of all types. The r^{-3} term is harder to rationalize because, apart from molecules with permanent dipoles, we would not expect a term proportional to r^{-3} in the true potential energy. However, here we are considering a model where the total energy is represented by effective interactions. Thus, one can simply view the r^{-3} term as a stand-in for all contributions to the energy that cannot be represented by the Lennard-Jones (9, 6) potential.

Following Parsafar and Mason [3] we assume that $r\approx v^{1/3}$. Substituting $r=v^{1/3}$ into Eq. (3) and differentiating, we obtain

$$\left(\frac{\partial(U/N)}{\partial v}\right)_T=-\left(\frac{D_9(T)}{v^4}+\frac{D_6(T)}{v^3}+\frac{D_3(T)}{v^2}\right) \quad (4)$$

where the $D_i(T)$ are temperature dependent. Since

$$P_i=\left(\frac{\partial u}{\partial v}\right)_T \quad (5)$$

By substituting Eq. (4) into Eq. (5)

$$P_i=-\left(\frac{D_9(T)}{v^4}+\frac{D_6(T)}{v^3}+\frac{D_3(T)}{v^2}\right) \quad (6)$$

Exact thermodynamic relation $P=T(\partial p/\partial T)_{\rho}-(\partial u/\partial v)_T$ can be written as

$$d\left(\frac{P}{T}\right)=\frac{P_i}{T^2}dT \quad (7)$$

Therefore,

$$\frac{P}{T}=A(T)\rho^4+B(T)\rho^3+C(T)\rho^2+d(\rho) \quad (8)$$

$d(\rho)$ has been arbitrarily chosen as the following function as $\rho=0$ at limit of P=0

$$d(\rho)=e\rho+f\rho^2+g\rho^3+h\rho^4 \quad (9)$$

Inserting Eq. (9) in Eq. (8) and rearranging provides a new regularity that is

$$(Z-1)v^3=A(T)+\frac{B(T)}{\rho}+\frac{C(T)}{\rho^2} \quad (10)$$

which implies a regularity should exist between $(Z-1)v^3$ and ρ in the form given by Eq. (10) at each temperature. For this reason we name the new EOS the isotherm regularity equation of state (IR EOS). The perspective we will adopt is that there is an equation (Eq. (10)) which can be correlated to the experimental data, and if a good fit is obtained the IR EOS can be used for density calculation. Eq. (10) can be written in the form of ρ for density calculation which is

$$A(T)\rho^4+B(T)\rho^3+C(T)\rho^2+\rho-\frac{P}{RT}=0 \quad (11)$$

Density has been calculated at different temperatures and pressures by Eq. (11) in gas, liquid and gas-liquid transition region. In derivation of IR EOS $(2Z-1)v^3$ was changed to $(Z-1)v^3$ because it was observed in the calculations that the factor 2 is unnecessary and even it can give inaccurate results in some cases of gases and gas-liquid transition region.

RESULTS AND DISCUSSION

GMA EOS gives good prediction for liquids at low and high pres-

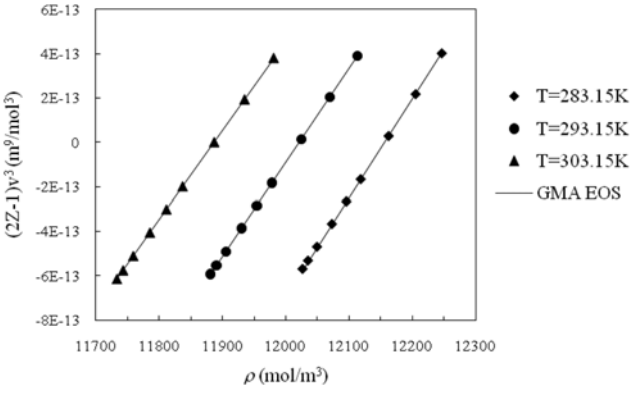

Fig. 1. Comparison of the experimental data of liquid DMC with GMA EOS for P=0.1 MPa to 25 MPa [19].

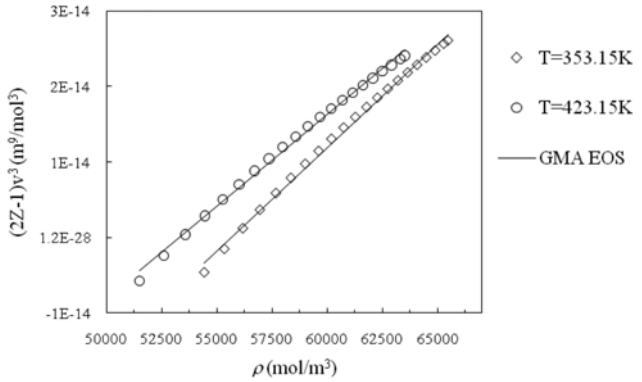

Fig. 2. Comparison of the experimental data of liquid water with GMA EOS for P=20 MPa to 800 MPa [26].

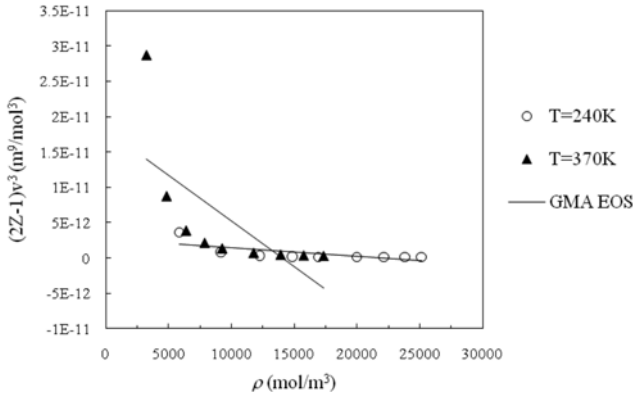

Fig. 3. Comparison of experimental data of gaseous oxygen with GMA EOS for P=10 MPa to 70 MPa [13].

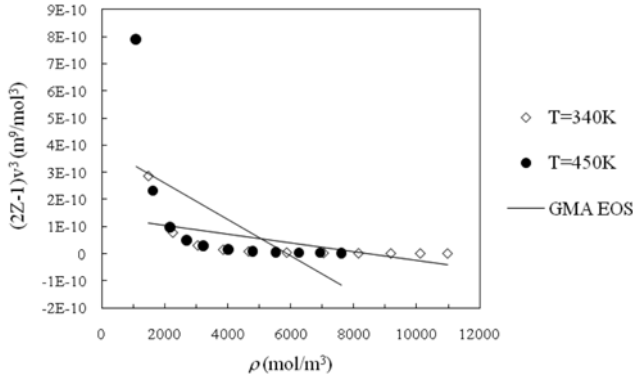

Fig. 4. Comparison of experimental data of gaseous methane with GMA EOS for P=2 MPa to 30 MPa [12].

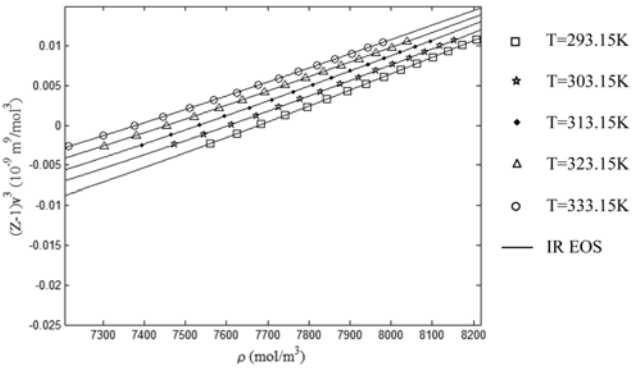

Fig. 5. Fitting isotherms of $(Z-1)v^3$ vs ρ for liquid Hexylamine for P=0.1 MPa to 140 MPa [22].

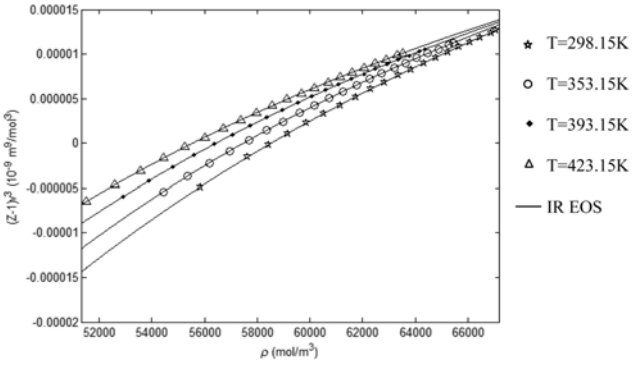

Fig. 6. Fitting isotherms of $(Z-1)v^3$ vs ρ for liquid water for P=20 MPa to 800 MPa [26].

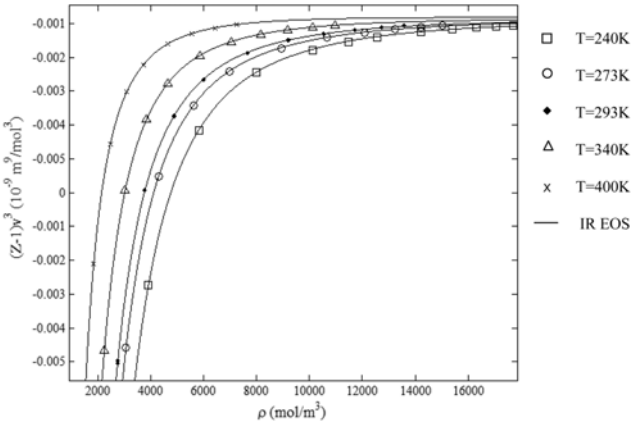

Fig. 7. Fitting isotherms of $(Z-1)v^3$ vs ρ for gaseous methane for P=2 MPa to 30 MPa [12].

sures. Fig. 1 shows that a linear relation exists between $(2Z-1)v^3$ and ρ for liquid dimethyl carbonate (DMC). This regularity also exists for liquid water up to very high pressures (800 MPa) with minor deviation from straight line (Fig. 2). In these figures experimental points and GMA EOS fits are shown by marks and lines, respectively. Nevertheless, GMA EOS cannot be used for calculation of gas density because a linear relation was not observed in this case. Experimental data of oxygen and methane in gas region were used and a linear relation between $(2Z-1)v^3$ and ρ at different temperatures was not observed (Fig. 3 and 4).

In spite of GMA EOS, the IR EOS can fit experimental data in liquid and gas regions at low and high pressures. Figs. 5-8 show experimental isotherms of $(Z-1)v^3$ versus ρ for liquid hexylamine, liquid water, gaseous methane and gaseous oxygen, as well as fit of $(Z-1)v^3$ versus ρ to the experimental points. As the figures show, $(Z-1)v^3$ versus ρ can fit experimental data very well in gas and liquid

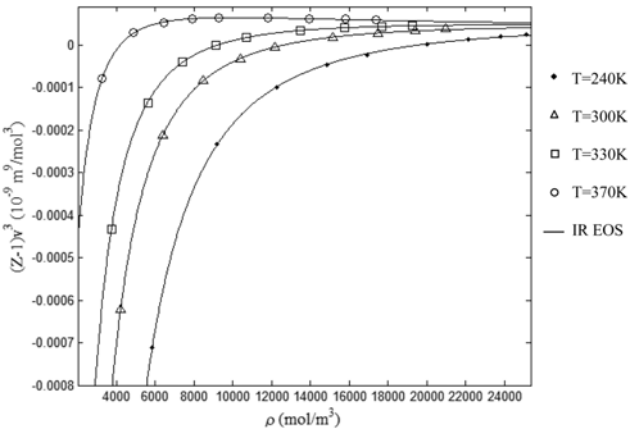

Fig. 8. Fitting isotherms of $(Z-1)v^3$ vs ρ for gaseous oxygen for P= 10 MPa to 70 MPa [13].

region. Fig. 9 shows fit of $(Z-1)v^3$ versus ρ to experimental ones for ethane, carbon dioxide, xenon and ethylene in gas-liquid transition region, and good agreement between experimental points and theory is observed. In Fig. 9 the liquid and gas regions are maximized in separate sections for better view of fitting. As these figures show, before transition points the IR EOS fits experimental data well, but after transition points it fits experimental data with less accuracy, which might be related to additional intermolecular potentials that were neglected in this study.

In fact, if a wide enough density range is considered, the isotherm regularity in the form of GMA cannot fit experimental data especially at low density region. The function $(Z-1)v^3$ versus density has a curvature and it is obvious that GMA EOS cannot describe this behavior. On the other hand, IR EOS gives an excellent fit over the entire density range. Some insight into the possible reason for this behavior can be explained by expanding the van der Waals expression for $(Z-1)v^3$ to obtain

$$(Z-1)v^3 = b^3 + b^4\rho + \frac{b^2}{\rho} + \left(b - \frac{a}{RT}\right)\frac{1}{\rho^2} + \cdots \tag{12}$$

where b and a are the usual van der Waals parameters associated with repulsive and attractive interactions, respectively. We note that a term linear in ρ appears in the equation if the other terms can be neglected. The terms proportional to $1/\rho$ and $1/\rho^2$ are interesting, because they can be neglected in liquid region due to high density. However, this simplification cannot be justified for the gas region and the contribution of $1/\rho$ and $1/\rho^2$ terms must be taken into account. For this reason a linear isotherm regularity appears insufficient to fit experimental data for low density region.

The isotherm regularity between $(Z-1)v^3$ versus ρ was correlated for 24 components at different states, and their density was calculated by Eq. (11) from low to high pressure. The list of these components is given in Tables 1-3, which includes polar and nonpolar components. The data in Table 1, 2 and 3 include components

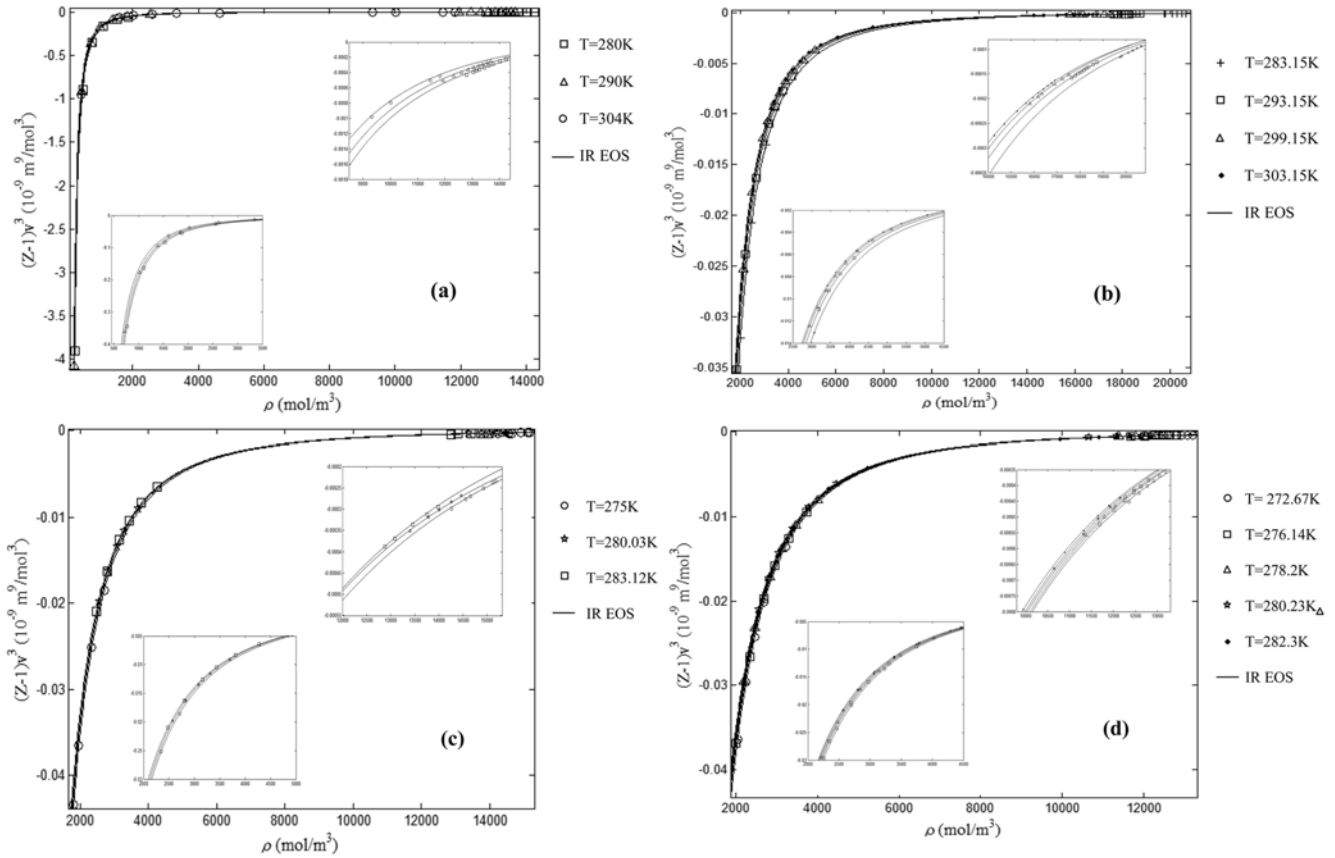

Fig. 9. Fitting isotherms of $(Z-1)v^3$ vs ρ in gas-liquid transition region for (a) Ethane for P=1 MPa to 12 MPa [28] (b) CO_2 for P=3.5 MPa to 9 MPa [27] (c) xenon for P=3 MPa to 6.45 MPa [29] (d) ethylene for P=3 MPa to 6 MPa [29].

Table 1. Percentage of AAD and SD between densities calculated by IR EOS and experimental data for components in gas region at different temperatures and pressures

Component	ΔT (K)	ΔP (MPa)	State	R^{2a}	NP[b]	% AAD[c]	SD[d]	Ref.
Argon	235-520	2-30	Gas	1	102	0.06	0.028	[11]
Nitrogen	240-520	1-30	Gas	0.99	127	0.04	0.013	[11]
Methane	240-520	2-30	Gas	1	127	0.26	0.104	[12]
Oxygen	200-370	10-70	Gas	0.99	63	0.25	0.102	[13]
Hydrogen	200-370	10-70	Gas	1	72	0.02	0.005	[13]
Natural gas	253.15-323.15	1-15	Gas	1	28	0.08	0.012	[14]
Neon	100-298	20-1000	Gas	0.99	21	0.16	0.173	[15]
Carbon monoxide	308.15-573.15	150-1000	Gas	0.99	48	0.01	0.005	[16]
Propene	373.15-473.15	100-1000	Gas	0.99	56	0.03	0.007	[17]

[a]R^2 rquare of the correlation coefficient of Eq. (10)

[b]NP=number of experimental points

[c]$\%\mathrm{AAD} = \sum \left| \frac{c_{exp} - c_{cal}}{c_{exp}} \right| \times 100$

[d] $\mathrm{SD} = \left[\frac{r}{NP-1} \sum (\rho_{exp} - \rho_{cal})^2 \right]^{0.3}$ where SD is in mol L^{-1}

Table 2. Percentage of AAD and SD between densities calculated by IR EOS and experimental data for components in liquid region at different temperatures and pressures

Component	ΔT (K)	ΔP (MPa)	State	R^{2a}	NP[b]	%AAD[c]	SD[d]	Ref.
Decane	283.15-328.15	0.1-40	Liquid	1	90	0.03	0.003	[18]
DMC	278.15-353.15	0.1-25	Liquid	1	81	0.05	0.009	[19]
Ethyl Acetate	298.15-393.15	0.1-35	Liquid	0.99	92	0.04	0.005	[20]
Butane	280-380	1-200	Liquid	0.99	112	0.07	0.013	[21]
Hexylamine	293.15-353.15	0.1-140	Liquid	1	105	0.02	0.003	[22]
[C2eim][Tf2N]	293.15-393.15	0.1-35	Liquid	0.99	80	0.09	0.004	[23]
1-Butanol	313.1-362.68	1-25	Liquid	1	147	0.08	0.011	[24]
Octanoic acid	293.15-323.15	0.1-25	Liquid	0.99	56	0.20	0.013	[25]
Water	298.15-423.15	20-800	Liquid	1	146	0.01	0.005	[26]
Mercury	303.15-423.15	100-800	Liquid	1	80	0.02	0.014	[26]

[a]R^2 rquare of the correlation coefficient of Eq. (10)

[b]NP=number of experimental points

[c]$\%\mathrm{AAD} = \sum \left| \frac{c_{exp} - c_{cal}}{c_{exp}} \right| \times 100$

[d] $\mathrm{SD} = \left[\frac{r}{NP-1} \sum (\rho_{exp} - \rho_{cal})^2 \right]^{0.3}$ where SD is in mol L^{-1}

Table 3. Percentage of AAD between densities calculated by IR EOS and experimental data for components in gas-liquid transition region at different temperatures and pressures

Component	ΔT (K)	ΔP (MPa)	State	R^{2a}	NP[b]	% AAD[c]	SD[d]	Ref.
CO_2	283.15-303.15	3.5-9	Gas-liquid region	1	105	0.59	0.140	[27]
Ethane	240-304	0.5-12	Gas-liquid region	1	117	1.02	0.281	[28]
Ethylene	272.67-282.3	3-6	Gas-liquid region	1	55	0.88	0.169	[29]
Xenon	275-286.94	3-6.45	Gas-liquid region	1	42	0.79	0.289	[29]
Propane	300-340	0.2-12	Gas-liquid region	1	27	1.27	0.224	[30]

[a]R^2 rquare of the correlation coefficient of Eq. (10)

[b]NP=number of experimental points

[c]$\%\mathrm{AAD} = \sum \left| \frac{c_{exp} - c_{cal}}{c_{exp}} \right| \times 100$

[d] $\mathrm{SD} = \left[\frac{r}{NP-1} \sum (\rho_{exp} - \rho_{cal})^2 \right]^{0.3}$ where SD is in mol L^{-1}

in gas, liquid and gas-liquid transition regions, which were chosen from available literature. Special attention was given to high pressure experimental data. The range of temperature and pressure of experimental data, component state, square of the correlation coefficient R^2 of Eq. (10), the number of experimental data, the average absolute deviations (AAD) of the calculated densities and the standard deviation (SD) are also given in these Tables. A complete set of densities calculated by IR EOS is given in supplementary data including A, B and C coefficients for each component. It appears that IR EOS predicts densities of liquids and gases from low to very high pressures well, but more deviations are observed in the gas-liquid transition region.

To confirm the reliability of the IR EOS, the PρT relations of liquids and gases are calculated and compared to experimental data. For example, the densities of carbon monoxide, oxygen and methane in gas region are compared to experimental data in Figs. 10-12. One of the improvements of IR EOS is density calculation of components in the gas region, which cannot be achieved by GMA EOS. To verify the density prediction capability of IR EOS, a compari-

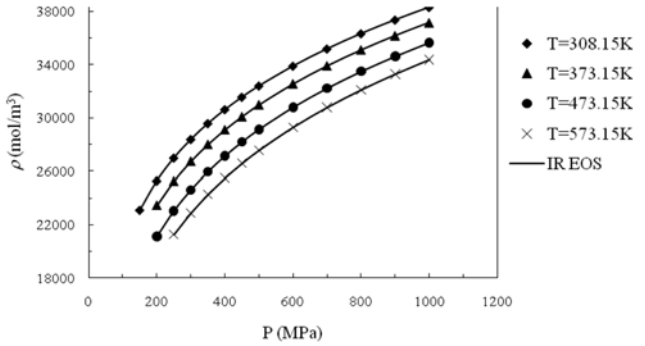

Fig. 10. Comparison of IR EOS density results with experimental data of carbon monoxide at gas region.

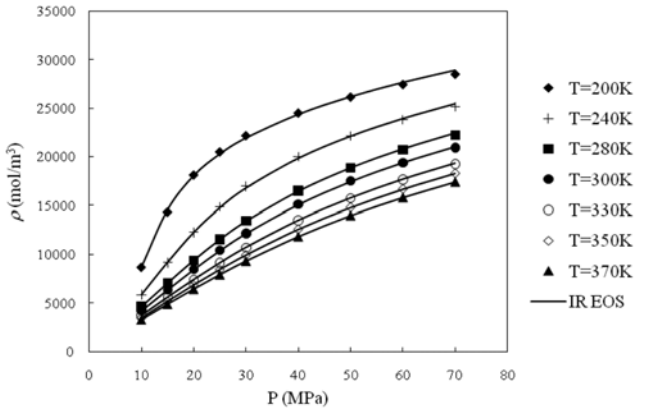

Fig. 11. Comparison of IR EOS density results with experimental data of oxygen at gas region.

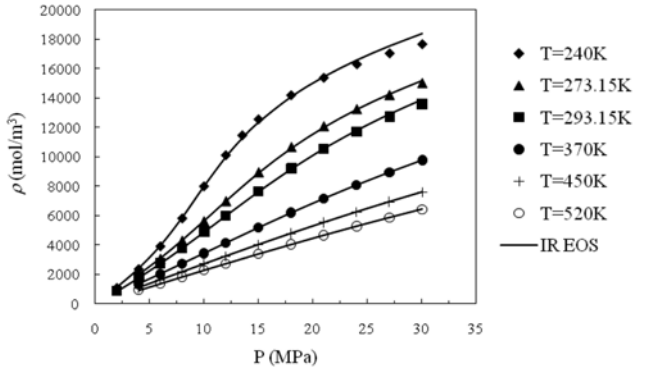

Fig. 12. Comparison of IR EOS density results with experimental data of methane at gas region.

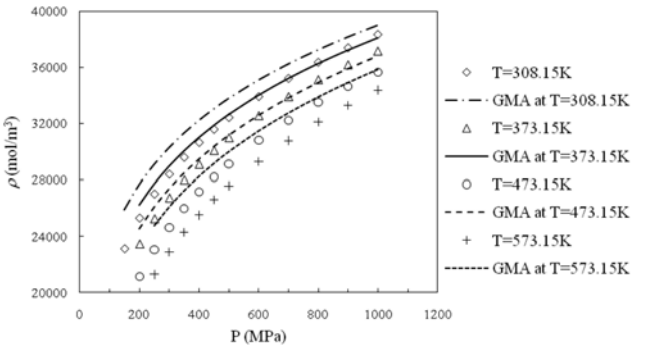

Fig. 13. Comparison of GMA EOS density results with experimental data of carbon monoxide at gas region.

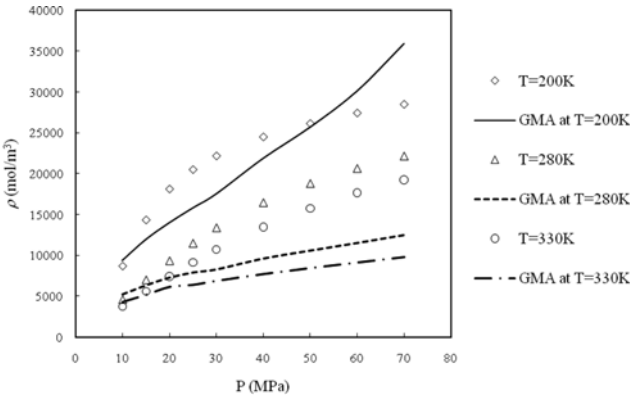

Fig. 14. Comparison of GMA EOS density results with experimental data of oxygen at gas region.

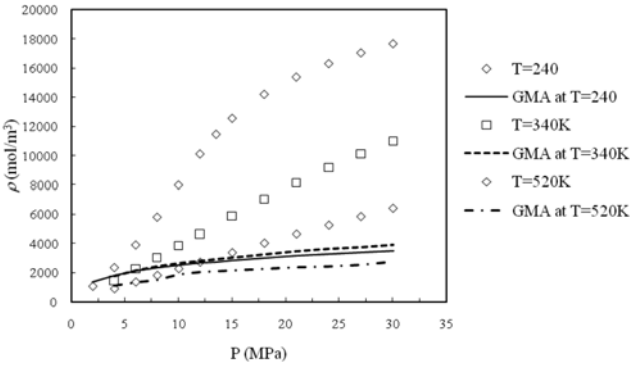

Fig. 15. Comparison of GMA EOS density results with experimental data of methane at gas region.

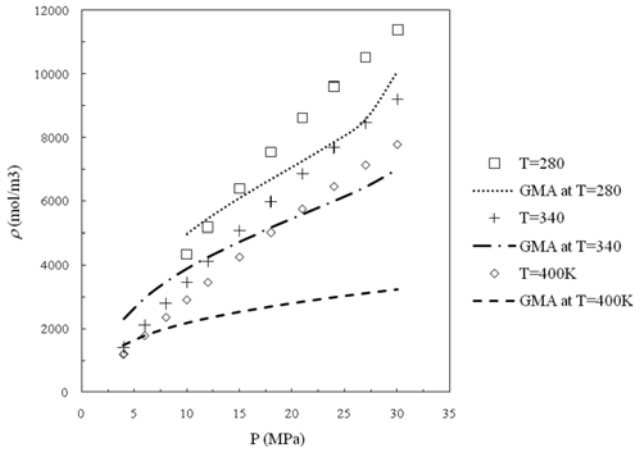

Fig. 16. Comparison of GMA EOS density results with experimental data of nitrogen at gas region.

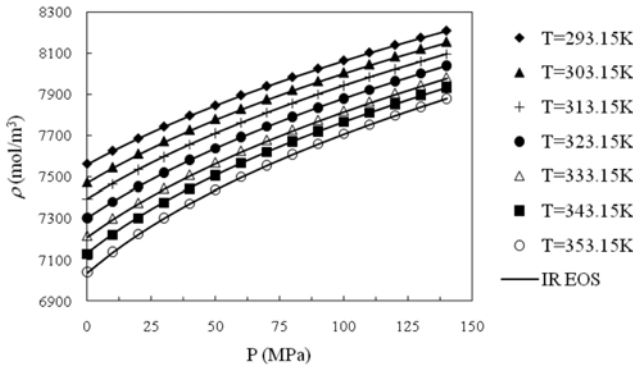

Fig. 17. Comparison of IR EOS density results with experimental data of liquid hexylamine.

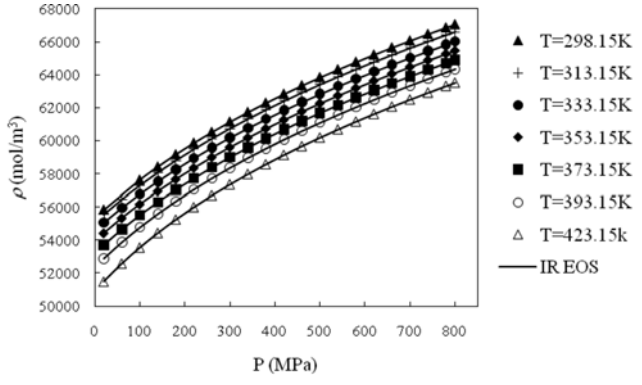

Fig. 18. Comparison of IR EOS density results with experimental data of liquid water.

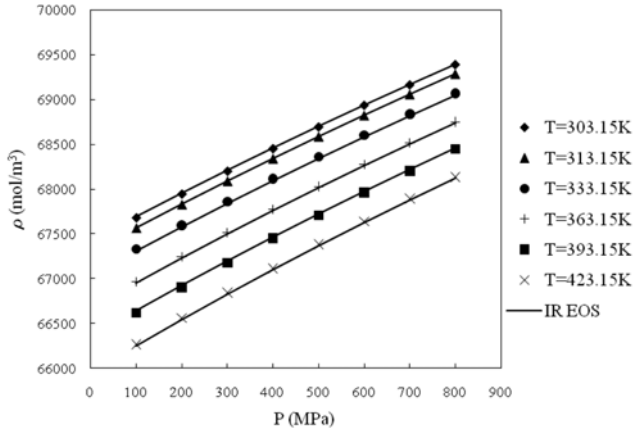

Fig. 19. Comparison of IR EOS density results with experimental data of liquid mercury.

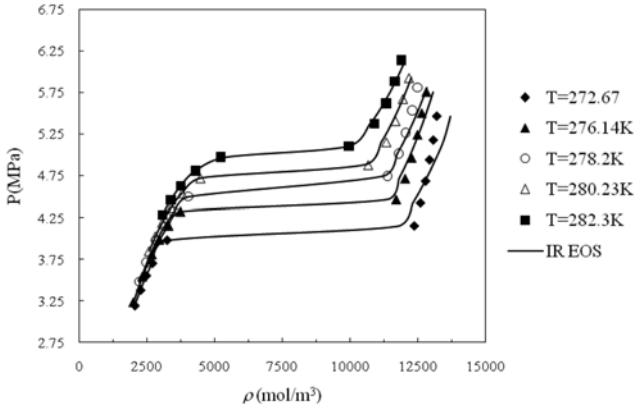

Fig. 20. Comparison of IR EOS density results with experimental data of ethylene in gas-liquid transition region.

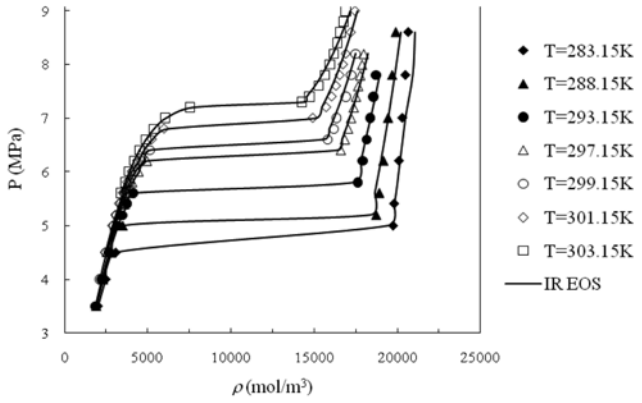

Fig. 21. Comparison of IR EOS density results with experimental data of carbon dioxide in gas-liquid transition region.

son between GMA and IR EOS for data of gas region has also been done. Therefore, densities of carbon monoxide, oxygen, methane (which were shown in Figs. 10-12) and nitrogen in gas phase are also calculated by GMA EOS and compared with experimental data in Figs. 13-16. As can be seen, great disagreement between GMA EOS and experimental data exists. In Figs. 17-19 the densities of liquid hexylamine, water and mercury are compared to IR EOS and the densities of ethylene and carbon dioxide in gas-liquid region are compared to IR EOS results in Figs. 20 and 21.

We have also calculated saturated liquid and vapor densities of five components of Table 3 by IR EOS, and the AADs are reported in Table 4. Above the transition point, the EOS gives AAD in calculated densities typically in the range of 1%-4% for selected com-

Table 4. Percentage of AAD between experimental and IR EOS calculated saturated liquid and vapour densities

Component	% AAD	
	Saturated liquid	Saturated gas
Propane	4.29	0.03
Ethane	4.04	2.33
Xenon	1.59	1.25
Ethylene	2.21	1.05
CO_2	1.37	0.99

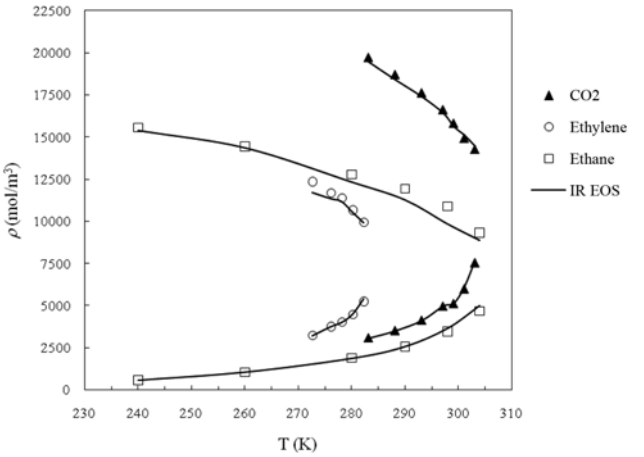

Fig. 22. Comparison of IR EOS calculated saturated liquid (upper curve) and saturated vapor (lower curve) densities with experimental data for carbon dioxide, ethylene and ethane.

ponents, while below the transition point (gas region) the EOS results are better. In other words, the EOS predictions for saturated vapor are better than saturated liquid. For accurate description of gas-liquid transition, more intermolecular forces must be taken into account. The problem with liquids is that there are many different kinds of interactions occurring simultaneously together with disperse attractions, especially the role of short-range interactions becomes more important. As a result, many specific terms must be invoked to describe these many specific interactions. If all the interactions were to be treated in their entirety, the resulting model would be too heavy to be of any practical use. Therefore, we have made approximation and used just three terms in potential energy for gas-liquid transition region description as other regions.

The saturated liquid and vapor densities of carbon dioxide, ethylene and ethane are compared to IR EOS calculations in Fig. 22, and more deviation in liquid region is observed. We conclude from the foregoing comparison that the present EOS is very accurate in homogeneous gas and liquid region for density calculation.

To complete model accuracy, comparison between calculated densities and experimental data at different temperatures up to high pressures was performed for all components, and percent of deviation was given in supplementary data where some of them are given below. The percentage of deviation between calculated and experimental density of nitrogen in gas phase is shown in Table 5. Also, the percentage of deviation between the experimental and IR EOS calculated densities for gaseous carbon monoxide, liquid mercury,

Table 5. Percentage of deviation between densities calculated by IR EOS and experimental data of nitrogen in gas phase

T (K)	P (MPa)	ρ_{exp} (mol/m^3)	ρ_{cal} (mol/m^3)	$\%\frac{\rho_{exp}-\rho_{cal}}{\rho_{exp}}$
240	2.00283	1022.40	1022.41	−0.001
	6.00723	3153.17	3153.64	−0.015
	10.0050	5313.71	5311.45	0.043
	12.0101	6371.24	6365.41	0.092
	15.0168	7883.91	7871.55	0.157
	18.0138	9275.17	9260.15	0.162
	21.0132	10536.5	10528.5	0.076
	24.0400	11677.6	11690.3	−0.109
	27.0308	12685.0	12732.8	−0.377
	30.0343	13590.9	13687.4	−0.710
440	3.99975	1077.15	1077.15	0.000
	4.01647	1081.59	1081.58	0.001
	6.00631	1604.26	1604.24	0.001
	8.00744	2120.14	2120.17	−0.001
	10.0265	2630.27	2630.33	−0.002
	12.0051	3119.65	3119.70	−0.002
	15.0084	3841.83	3841.83	0.000
	18.0059	4537.33	4537.07	0.006
	21.0102	5208.44	5208.08	0.007
	24.0147	5853.77	5853.44	0.006
	27.0178	6473.51	6473.27	0.004
	30.0163	7067.55	7067.70	−0.002
520	4.00389	910.539	910.539	0.000
	6.01250	1355.20	1355.21	−0.001
	8.02154	1791.59	1791.60	−0.001
	10.0262	2218.56	2218.54	0.001
	12.0265	2636.08	2635.99	0.003
	15.0105	3242.94	3242.78	0.005
	18.0055	3832.92	3832.63	0.008
	21.0046	4404.36	4404.27	0.002
	24.0214	4960.16	4960.44	−0.006
	27.016	5493.30	5494.32	−0.019
	30.0264	6011.09	6013.83	−0.046

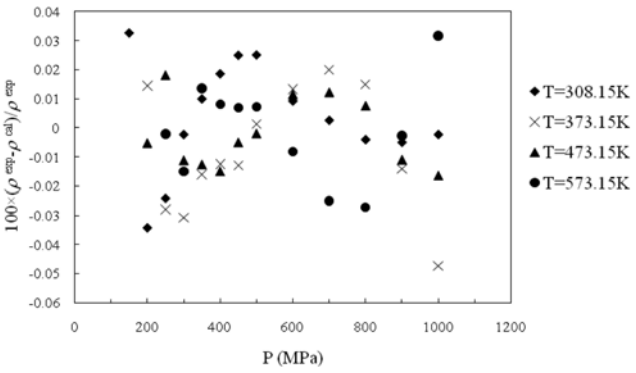

Fig. 23. Percentage of deviations between the experimental and IR EOS calculated density of carbon monoxide in gas region.

ethylene and carbon dioxide (in gas-liquid transition region) are presented in Figs. 23-26. In Figs. 25 and 26 (gas-liquid transition) more deviation can be observed when the liquid region is reached, while

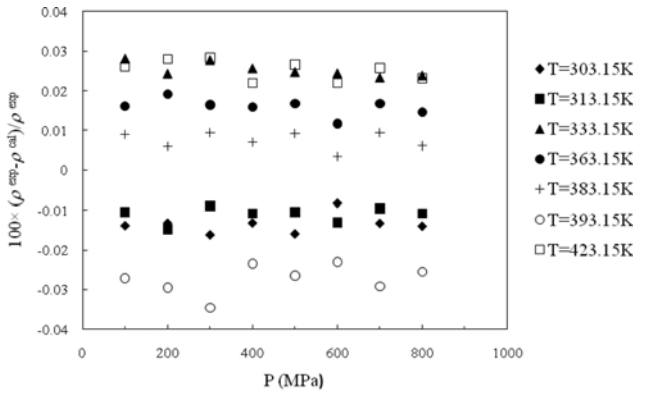

Fig. 24. Percentage of deviations between the experimental and IR EOS calculated density of mercury in liquid region.

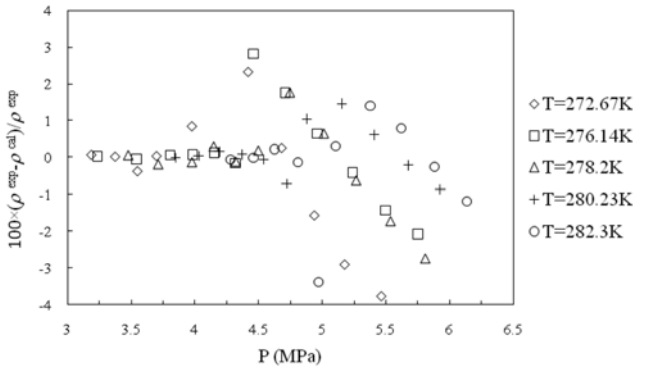

Fig. 25. Percentage of deviations between the experimental and IR EOS calculated density of ethylene in gas-liquid region.

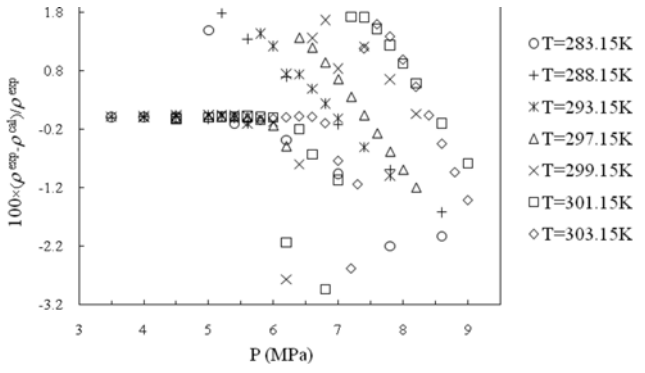

Fig. 26. Percentage of deviations between the experimental and IR EOS calculated density of carbon dioxide in gas-liquid region.

deviations in gas region are very low.

CONCLUSIONS

We have proposed a new EOS for gases and liquids that is suitable for high pressure calculation of density. The capability of this EOS to predict densities has been demonstrated and compared with experimental data. The EOS is based on intermolecular potential energy and the parameters are determined by fitting isothermal regularity to experimental data. The EOS is a nonlinear regularity as it contains two density-dependent terms with three adjustable parameters. The EOS predictions are good in the homogeneous gas and liquid regions. Nevertheless, it gives less accurate results in gas-liquid transition region, which might be related to additional intermolecular potentials that were neglected in this study because these corrections might add more complexity to the EOS.

REFERENCES

1. J. Hwang, C. H. Kim and G. B. Lim, *Korean J. Chem. Eng.*, **12**, 244 (1995).
2. J. S. Lim, C. H. Yoon and K. P. Yoo, *Korean J. Chem. Eng.*, **26**, 1754 (2009).
3. G. Parsafar and E. A. Mason, *J. Phys. Chem.*, **97**, 9048 (1993).
4. M. H. Ghatee and M. J. Bahadori, *J. Phys. Chem. B*, **105**, 11256 (2001).
5. E. K. Goharshadi, A. Morsali and M. Abbaspour, *Fluid Phase Equilibr.*, **230**, 170 (2005).
6. E. K. Goharshadi and F. Moosavi, *Fluid Phase Equilibr.*, **238**, 112 (2005).
7. E. K. Goharshadi and M. Abareshi, *Fluid Phase Equilibr.*, **268**, 61 (2008).
8. E. K. Goharshadi and M. Moosavi, *Ind. Eng. Chem. Res.*, **44**, 6973 (2005).
9. M. Moosavi and E. K. Goharshadi, *Int. J. Thermophys.*, **27**, 1515 (2006).
10. E. K. Goharshadi and M. Moosavi, *J. Mol. Liq.*, **142**, 41 (2008).
11. J. Klimeck, R. Kleinrahm and W. Wagner, *J. Chem. Thermodyn.*, **30**, 1571 (1998).
12. J. Klimeck, R. Kleinrahm and W. Wagner, *J. Chem. Thermodyn.*, **33**, 251 (2001).
13. B. A. Younglove and N. A. Olien, Tables of Industrial Gas Container Contents and Density for Oxygen, Argon, Nitrogen, Helium, and Hydrogen, National Bureau of Standards Technical Note 1079, Washington (1985).
14. L. Capla, P. Buryan, J. Jedelsky, M. Rottner and J. Linek, *J. Chem. Thermodyn.*, **34**, 657 (2002).
15. R. Eggenberger, S. Gerber, H. Huber, D. Searles and M. Welker, *J. Chem. Phys.*, **99**, 9163 (1993).
16. S. L. Robertson and S. E. Babb, *J. Chem. Phys.*, **53**, 1094 (1970).
17. S. L. Robertson and S. E. Babb, *J. Chem. Phys.*, **51**, 1357 (1969).
18. J. Troncoso, D. Bessiéres, C. A. Cerdeiriña, E. Carballo and L. Romaní, *J. Chem. Eng. Data*, **49**, 923 (2004).
19. L. Lugo, M. J. P. Comuñas, E. R. López and J. Fernández, *Fluid Phase Equilibr.*, **186**, 235 (2001).
20. R. L. Gardas, I. Johnson, D. M. D. Vaz, I. M. A. Fonseca and A. G. M. Ferreira, *J. Chem. Eng. Data*, **52**, 737 (2007).
21. H. Miyamoto and M. Uematsu, *J. Chem. Thermodyn.*, **39**, 588 (2007).
22. Y. Miyake, A. Baylaucq, F. Plantier, D. Bessiéres, H. Ushiki and C. Boned, *J. Chem. Thermodyn.*, **40**, 836 (2008).
23. L. I. N. Tome, P. J. Carvalho, M. G. Freire, I. M. Marrucho, I. M. A. Fonseca, A. G. M. Ferreira, J. A. P. Coutinho and R. L. J. Gardas, *J. Chem. Eng. Data*, **53**, 1914 (2008).
24. A. Z. Moreno, L. A. G. Luna and L. E. C. Camacho, *J. Chem. Ther-*

modyn., **39**, 254 (2007).
25. W. T. Vong and F. N. Tsai, *J. Chem. Eng. Data*, **42**, 1116 (1997).
26. T. Grindley and J. E. Lind, *J. Chem. Phys*., **54**, 3983 (1971).
27. R. B. Gupta and J. J. Shim, Solubility in Supercritical Carbon Dioxide, CRC Press, Florida (2007).
28. M. Funke, R. Kleinrahm and W. Wagner, *J. Chem. Thermodyn*., **34**, 2001 (2002).
29. C. M. M. Duarte, H. J. R. Guedes and M. N. da Ponte, *J. Chem. Thermodyn*., **32**, 891 (2000).
30. S. Glos, R. Kleinrahm and W. Wagner, *J. Chem. Thermodyn*., **36**, 1037 (2004).